J Mater Sci: Mater Electron (2017) 28:18686–18696
DOI 10.1007/s10854-017-7818-1

Synthesis and photoluminescence enhancement of $Ca_3Sr_3(VO_4)_4$:Eu^{3+} red phosphors by Sm^{3+} doping for white LEDs

Qinxue Tang[1] · Kehui Qiu[1,2] · Junfeng Li[2] · Wentao Zhang[1] · Yu Zeng[1]

Received: 24 April 2017 / Accepted: 29 August 2017 / Published online: 4 September 2017

Abstract A new type of red-emitting Eu^{3+} and Sm^{3+} co-doped $Ca_3Sr_3(VO_4)_4$ phosphor was synthesized by the combustion method. The photoluminescence properties and microstructure were investigated by photoluminescence spectroscopy, X-ray powder diffraction, and scanning electron microscopy. All samples were found to match perfectly with the rhombohedral structure and belong to the *R*3*c* space group. The photoluminescence emission intensity of the optimal phosphor $Ca_3Sr_3(VO_4)_4$:0.05Eu^{3+}, 0.09Sm^{3+} at 619 nm was significantly enhanced compared with those of $Ca_3Sr_3(VO_4)_4$:Eu^{3+} samples and commercial Y_2O_3:Eu^{3+} at an excitation wavelength of 393 nm, as a result of the energy transfer from Sm^{3+} to Eu^{3+}. The energy transfer process between Sm^{3+} and Eu^{3+} is discussed and interpreted by considering the energy level diagram. Furthermore, the CIE chromaticity coordinate of $Ca_3Sr_3(VO_4)_4$:0.05Eu^{3+}, 0.09Sm^{3+} was closer to the standard red-emitting point ($x=0.67$, $y=0.33$) than Y_2O_3:Eu^{3+}. The luminescence performance of $Ca_3Sr_3(VO_4)_4$:Eu^{3+}, Sm^{3+} upon excitation by near-UV radiation makes it a promising red phosphor for manufacturing white-light-emitting diodes.

✉ Kehui Qiu
qkh2188@163.com

[1] College of Materials and Chemistry & Chemical Engineering, Chengdu University of Technology, Chengdu 610059, China

[2] Institute of Materials Science and Technology, Chengdu University of Technology, Chengdu 610059, China

1 Introduction

Rare-earth ions have been extensively used in various devices, such as scintillators [1], fluorescent lamps [2], and white LEDs [3]. Among these applications, white LEDs and Hg-free fluorescent lamps are considered to be eco-friendly. White LEDs have many merits, such as high efficiency, long operational lifetime, and compactness [4]. One conventional method to fabricate white light is using a yellow phosphor (typically YAG:Ce^{3+} [5, 6]) in combination with a blue-emitting InGaN LED chip. However, this approach leads to a high color temperature and is an imperfect match in terms of the color rendering in the red region, and it does not satisfy the requirements for low-color-temperature illumination [7]. Another approach is combining semiconductor chips of tri-color phosphors to fabricate white LEDs excited by one UV or near-UV (NUV) chip [8, 9]. The main advantages of this method are avoiding light loss in the process of white light emitting and controlling the emission intensity of different colors to obtain the desired output color [10–12]. However, the most common commercially available red-emitting phosphors, such as Y_2O_2S:Eu^{3+} and Y_2O_3:Eu^{3+}, are inefficient and chemically unstable. Therefore, new inorganic red-emitting phosphors need to be developed to combine with an appropriate NUV LED for signaling or illumination applications. In addition, the majority of commercial red-emitting phosphors at present use rare-earth elements as the positive ion in the host lattices (e.g., Y^{3+}, La^{3+}, Ga^{3+}), which means that the cost of red-emitting phosphors is much higher than those of yellow-emitting and blue-emitting phosphors.

Recently, solid-state phosphors based on vanadates doped with rare-earth ions have attracted increasing attention because they can be excited by a broad range of wavelengths and have stable chemical characteristics [13, 14]. In the vanadate group (VO_4^{3-}), four oxygen ions are

coordinated to a V^{5+} ion in a structure with tetrahedral symmetry, which is considered to be an effective luminescent center [15]. Because of the occurrence of energy transfer, the photoluminescence intensity of vanadate-based phosphors could be improved by doping trivalent rare-earth ions into the vanadate hosts. In particular, vanadate-based phosphors with doped Eu^{3+} have been investigated because they can be applied extensively in the solid-state luminescence industry [13]. Choi et al. [16] reported the solid-state synthesis of $Ca_3Sr_3(VO_4)_4$:Eu^{3+} and $Ca_3Sr_3(VO_4)_4$:Eu^{3+}, M^+ (M = Li, Na, K) red-emitting phosphors and studied the effects of Eu^{3+} concentration, the type of charge compensation, and their concentration on emission intensity. Sun et al. [17] reported the use of another solid-state reaction to synthesize $Ca_3Sr_3(VO_4)_4$:Sm^{3+}, Na^+ red-emitting phosphors. Comparing to conventional solid state reaction, the combustion method can be reacted at relatively low temperature [18]. It also has many advantages such as short reaction time, high efficiency of energy conservation and homogeneous grain size. To the best of our knowledge, there have been no reports of $Ca_3Sr_3(VO_4)_4$:Eu^{3+} red-emitting phosphors using Sm^{3+} co-doping for white LEDs. Sm^{3+} can be applied as the sensitizer in Eu^{3+}-doped phosphors and the excitation bands of Eu^{3+}-doped samples can be strengthened and broadened by Sm^{3+} doping in the range of ultraviolet–near ultraviolet (UV–NUV) [19]. Moreover, it has been reported that the energies of the $^4G_{5/2}$ energy level of Sm^{3+} and the $^5D_0$ energy level of Eu^{3+} are similar [20]. Thus, it seemed plausible that Sm^{3+} could transfer absorbed energy to Eu^{3+} in $Ca_3Sr_3(VO_4)_4$ phosphors and that the emission intensity could be improved significantly.

In this paper, the combustion method has been applied to synthesize $Ca_3Sr_3(VO_4)_4$:Eu^{3+}, Sm^{3+} phosphors for the first time, to the best of our knowledge. In addition, $Ca_3Sr_3(VO_4)_4$:Eu^{3+} and commercial Y_2O_3:Eu^{3+} phosphors have also been synthesized by the same method for comparison. The photoluminescence properties of Sm^{3+} and Eu^{3+} single-doped and co-doped samples were investigated and the relevant mechanism is analyzed.

2 Experimental

2.1 Sample preparation

The $Ca_3Sr_3(VO_4)_4$:Eu^{3+}, $Ca_3Sr_3(VO_4)_4$:Sm^{3+}, and $Ca_3Sr_3(VO_4)_4$:Eu^{3+}, Sm^{3+} phosphors were synthesized by the combustion method. The starting materials were high-purity europium oxide (Eu_2O_3), high-purity samarium oxide (Sm_2O_3), analytical reagent (AR) grade calcium carbonate ($CaCO_3$), AR grade strontium carbonate ($SrCO_3$), AR grade ammonium metavanadate (NH_4VO_3), nitric acid (HNO_3), and citric acid ($C_6H_8O_7{\cdot}H_2O$). The appropriate stoichiometric ratio of Eu_2O_3 and Sm_2O_3 was dissolved in 1 mL HNO_3 with 15 mL distilled water to afford a homogeneous solution. Then, $CaCO_3$, $SrCO_3$, $C_6H_8O_7{\cdot}H_2O$, and NH_4VO_3 were added to the solution with heating and stirring at a temperature of 70–80 °C. After stirring this solution for around 30 min, we obtained the blue sol precursor. This was placed into a furnace at a defined temperature for 1 h under an air atmosphere and then allowed to cool to room temperature.

2.2 Characterization

The crystal structures of the samples were determined by X-ray diffraction with Cu Kα radiation (Philips X'Pert Pro MPD, Cu Kα, 40 kV, 40 mA, λ = 1.5418 Å). The sample morphologies and particle sizes were investigated using a JEX-100CX scanning electron microscope with a running voltage of 10 kV. Excitation and emission spectra of all of the synthesized samples were recorded using a Hitachi F-7000 photoluminescence spectrometer. The fluorescence lifetime of the obtained samples was investigated using a fluorescence spectrophotometer (Fluorolog-3-Tau, Jobin Yvon Inc., USA). The absolute PL quantum yields (QYs) of powder samples were determined on a FLS980 (Eidinburgh) equipped with an integrating sphere. The fluorimeter have been corrected for the wavelength dependence of the sensitivity of the detectors and throughput of the monochromators. All samples were measured at room temperature.

3 Results and discussion

3.1 Synthesis temperature

To determine the optimum synthesis temperature, this parameter was varied while other experimental conditions were kept the same. The phase, degree of crystallinity, and photoluminescence properties of the samples obtained using various synthesis temperatures were investigated. The powder XRD patterns of the $Ca_3Sr_3(VO_4)_4$:Eu^{3+} phosphors obtained at four different synthesis temperatures (700, 800, 900, 1000 °C) are shown in Fig. 1. It can be seen that the diffraction peaks for all samples matched perfectly with the standard diffraction peaks for $Ca_3Sr_3(VO_4)_4$ (PDF card: JCPDS 52-0468), which has a rhombohedral structure. These results confirmed that all of the $Ca_3Sr_3(VO_4)_4$ samples synthesized here after firing at the various temperatures for 1 h were highly pure and belonged to the *R*3*c* space group, without the occurrence of other obvious mixed phases, and that Eu^{3+} entered into the crystal lattice of $Ca_3Sr_3(VO_4)_4$ without affecting the host structure. Taking the ion sizes of Sr^{3+} (0.118 nm), Ca^{3+} (0.1 nm), and Eu^{3+} (0.094 nm) and valence states into consideration, Eu^{3+} ions can easily

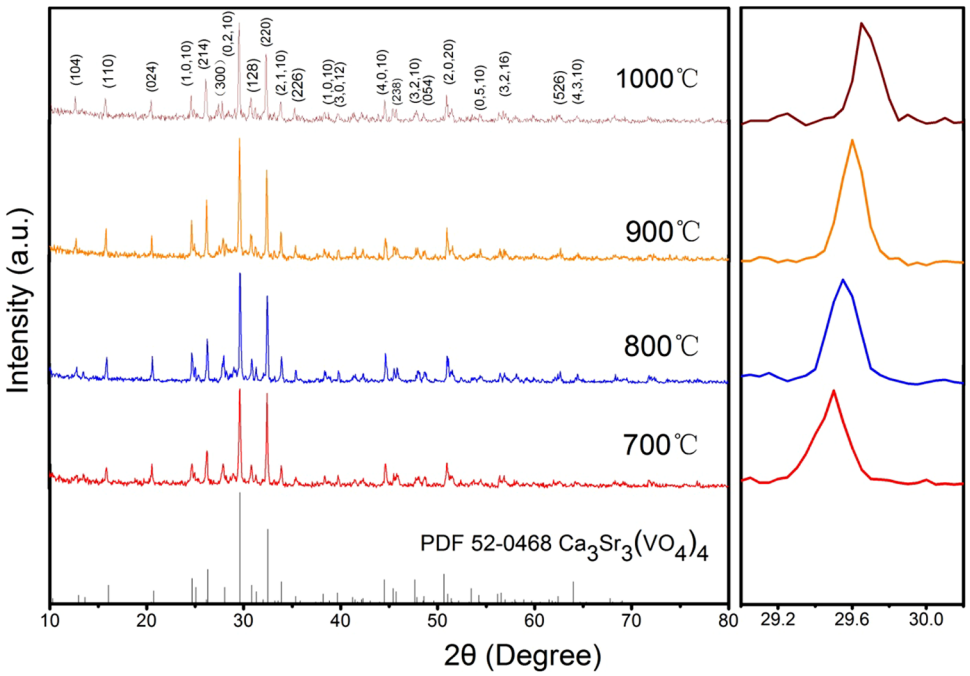

Fig. 1 X-ray diffraction patterns of the $Ca_3Sr_3(VO_4)_4$:Eu^{3+} samples obtained at different synthesis temperatures

substitute for Ca^{3+} ions in the $Ca_3Sr_3(VO_4)_4$ phosphor due to the similar ion radii. A small shifting of the predominant diffraction peaks around 29.6° (2θ) in the XRD patterns of the $Ca_3Sr_3(VO_4)_4$:Eu^{3+} samples was observed as shown in Fig. 1 right side. This further confirmed that the Eu^{3+} ions successfully replaced the Ca^{3+} ions in the host lattice. The shifting in the XRD patterns was due to the ionic radii difference between the Eu^{3+} ion and Ca^{3+} ion. With the increase of temperature from 700 to 900 °C, the intensity of diffraction peaks enhanced orderly and increasingly sharp and symmetrical, which indicates the enhancement of crystalline. It could be also observed from the magnified XRD predominant diffraction peaks in Fig. 1 that the XRD peak width declined orderly. Meanwhile, with the increase of the synthesis temperature from 700 to 1000 °C, the FWHM of the intense diffraction peaks (0, 2, 10) decreased orderly (0.190 at 700 °C, 0.169 at 800 °C, 0.155 at 900 °C, and 0.149 at 1000 °C), which can be calculated by the software of Jade. The FWHM results mean that the crystallinity and the grain size of samples were enhanced successively. The FWHM of the intense diffraction peaks were used to calculate the average crystallite sizes obtained at different synthesis temperatures by using the Scherrer equation:

$$D = \frac{K\lambda}{\beta \cos\theta} \quad (1)$$

where D is the average crystallite size, K (K = 0.89) is the Scherrer constant, $\lambda$is the wavelength of the X-ray, $\beta$is the FWHM of the intense diffraction peaks (0, 2, 10) and θ is the diffraction angle of the intense diffraction peaks. According to this equation, the average crystallite sizes of $Ca_3Sr_3(VO_4)_4$:Eu^{3+} phosphors synthesized at 700, 800, 900, 1000 °C were 47.55, 53.49, 58.26 and 60.64 nm, respectively. Compared with the solid-state reaction method, highly purified and crystalline $Ca_3Sr_3(VO_4)_4$:Eu^{3+} phosphors can be obtained by the citric acid assisted solution combustion method at relatively lower synthetic temperatures [18]; the reason for this is that the precursor of the citric acid assisted sol combustion method is the sol system, and it is possible that the strong exothermic action can occur quickly and easily at synthesis temperatures of 700–900 °C [21].

The synthesis temperature affects the grain size and this in turn affects the photoluminescence properties of phosphors [22, 23]. Figure 2 shows the SEM images of the samples synthesized at the various temperatures. The sample synthesized at 700 °C (Fig. 2a) did not exhibit a homogenous size distribution and some particles gathered together, because the synthesis temperature was too low and the combustion reaction was insufficient. The samples synthesized at 800–1000 °C (Fig. 2b–d) exhibited homogenous size distributions and the particle size grew quickly with the increasing synthesis temperature. The grain diameters of the samples were approximately 200–300 nm at 700 °C, 400–500 nm at 800 °C, 600–800 nm at 900 °C, and over 1000 nm at 1000 °C.

Figure 3 shows the emission spectra of the $Ca_3Sr_3(VO_4)_4$:Eu^{3+} phosphors synthesized at the various temperatures, revealing that the synthesis temperature had little influence on the overall peak positions and shapes of the spectra of the four samples, although the relative peak intensities showed some differences. In particular, it can be seen that for the samples obtained at different synthesis

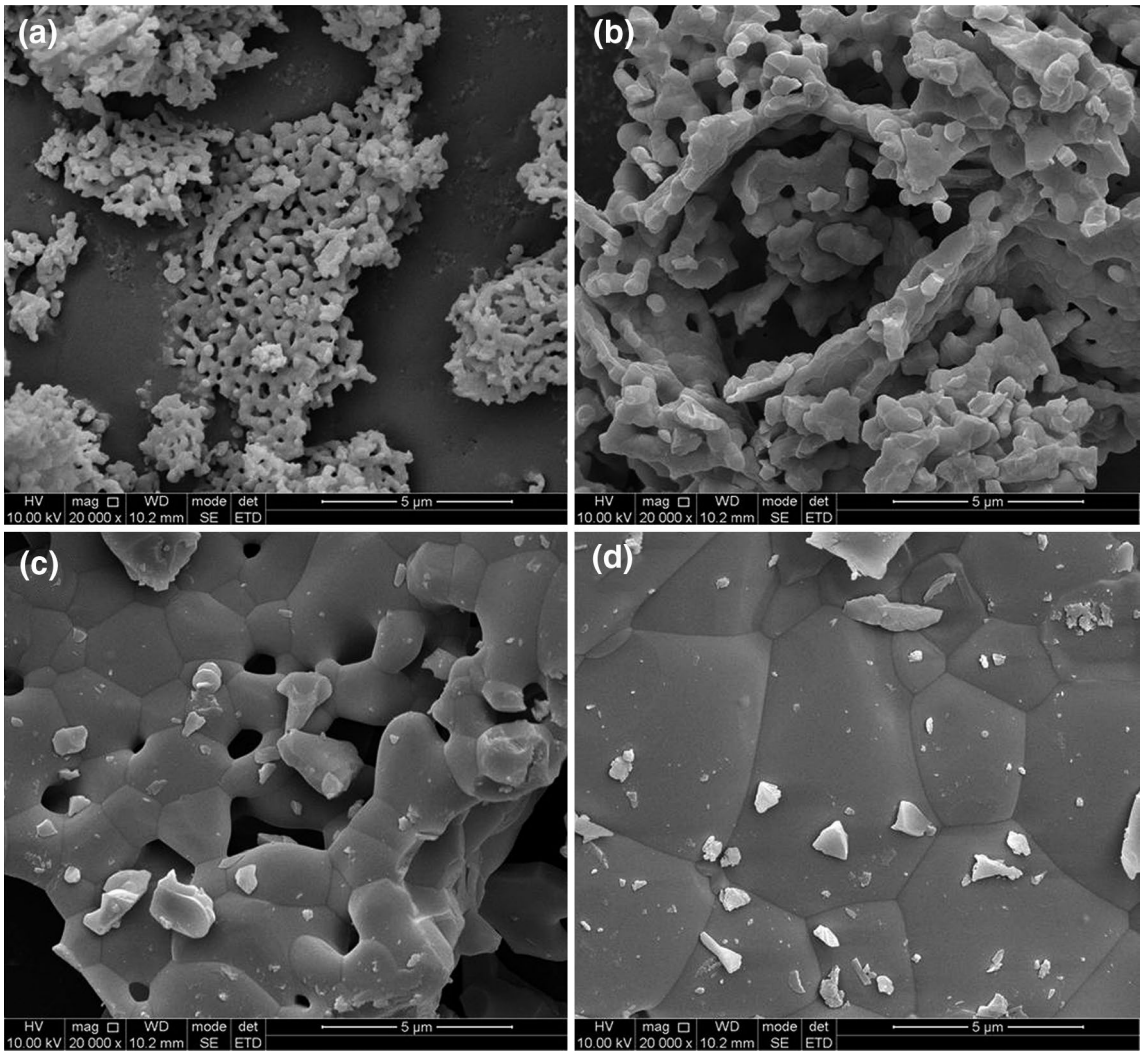

Fig. 2 SEM images of the samples synthesized at different temperatures: **a** 700 °C, **b** 800 °C, **c** 900 °C, **d** 1000 °C

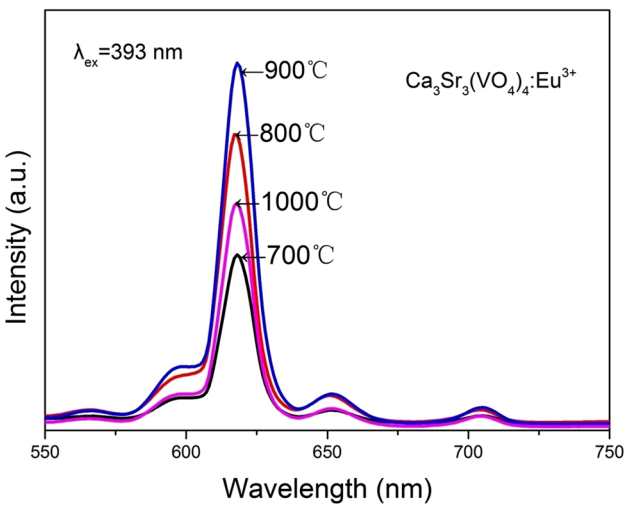

Fig. 3 Emission spectra of the $Ca_3Sr_3(VO_4)_4$:0.05Eu^{3+} samples prepared at different temperatures

temperatures, the intensities of the main emission peak at 619 nm were different. From 700 to 900 °C, higher synthesis temperatures led to stronger emission spectra, and the red emission intensity was strongest at a synthesis temperature of 900 °C. Upon further increasing the synthesis temperature to 1000 °C, the red emission intensity decreased.

The reason for this phenomenon is that the crystallization of $Ca_3Sr_3(VO_4)_4$ structure is improved with the increasing temperature in the range of 700–900 °C and the grain boundary gradually decreased, and high temperature favors the doping Eu^{3+} ions into $Ca_3Sr_3(VO_4)_4$ lattice, which is consistent with the results shown in Figs. 1 and 2. What is more, as the particle size increases with the increasing temperature in the range of 700–900 °C, stable site for the active ion could be increased increasing emission intensity. However, upon further increasing the synthesis temperature to 1000 °C, agglomeration of active ions at the elevated temperature is the possible reason why the emission intensity decreased. Figure 4 shows the

Decay curves of the $Ca_3Sr_3(VO_4)_4$:Eu^{3+} samples obtained at different synthesis temperatures. The monitoring wavelength is at 619 nm with a 393 nm excitation. The decay curves of $Ca_3Sr_3(VO_4)_4$:Eu^{3+} phosphors are well fitted by the second order exponential function:

$$y = y_0 + A_1 \exp\left(\frac{-x - x_0}{\tau_1}\right) + A_2 \exp\left(\frac{-x - x_0}{\tau_2}\right) \quad (2)$$

where τ_1, and τ_2 are the luminescence decay times. The value of decay time can be calculated by the following equation [24]:

$$\tau = \frac{(A_1\tau_1^2 + A_2\tau_2^2)}{(A_1\tau_1 + A_2\tau_2)} \quad (3)$$

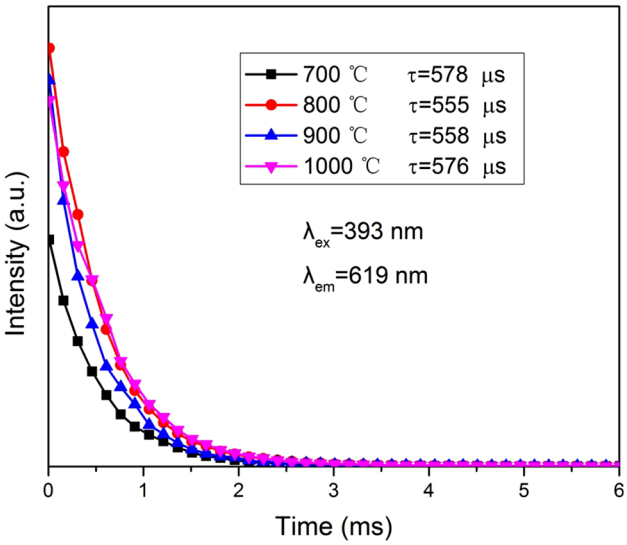

Fig. 4 Decay curves of the $Ca_3Sr_3(VO_4)_4$:Eu^{3+} samples obtained at different synthesis temperatures

The values of decay time of $Ca_3Sr_3(VO_4)_4$:Eu^{3+} phosphors synthesized at 700, 800, 900, 1000 °C were 578, 555, 558, 576 μs, respectively. It can be seen that the sintering temperature only has a slight influence on the luminescence lifetime, which indicates that the sintering temperature can effectively improve the emission intensity of samples in the range of 700–900 °C, but not change their luminescence lifetime. Therefore, the best photoluminescence properties for the Eu^{3+}-doped $Ca_3Sr_3(VO_4)_4$ phosphors were obtained at a synthesis temperature of 900 °C.

3.2 Photoluminescence spectra of Eu^{3+}/Sm^{3+}-doped $Ca_3Sr_3(VO_4)_4$

Figure 5 shows the photoluminescence (excitation and emission) spectra of $Ca_3Sr_3(VO_4)_4$:Eu^{3+}. The emission spectrum of $Ca_3Sr_3(VO_4)_4$:Eu^{3+}, using an excitation of 393 nm, exhibited several emission peaks centered at 594, 619, 651, and 705 nm, which correspond to the $^5D_0 \rightarrow {}^7F_J$ ($J = 1$, 2, 3, 4) transitions of Eu^{3+}, respectively. Of these peaks, the strongest peak was that situated at 619 nm derived from the $^5D_0 \rightarrow {}^7F_2$ transition, because Eu^{3+} occupies the D_{2d} site without inversion symmetry [25]. Upon monitoring the $^5D_0 \rightarrow {}^7F_2$ transition of Eu^{3+}, the region of excitation was found to extend from 200 to 500 nm, which included a broad charge transfer band (CTB) and a number of small sharp peaks. The CTB was centered at 285 nm, which is mainly from the allowed transition $^1A_1 \rightarrow {}^1T_2$ with the charge transfer states (CTS) of VO^{3-} [26]. Multiple sharp peaks could be observed from 350 to 500 nm, which was due to the f–f inner-shell transitions of Eu^{3+}, regardless of the concentration of Eu^{3+}, and these sharp peaks located at 360, 380, 393, 415, and 463 nm were assigned to the $^7F_0 \rightarrow {}^5D_4$, $^5L_7$, $^5L_6$, $^5D_3$, and $^5D_2$ transitions of Eu^{3+}, respectively. The most

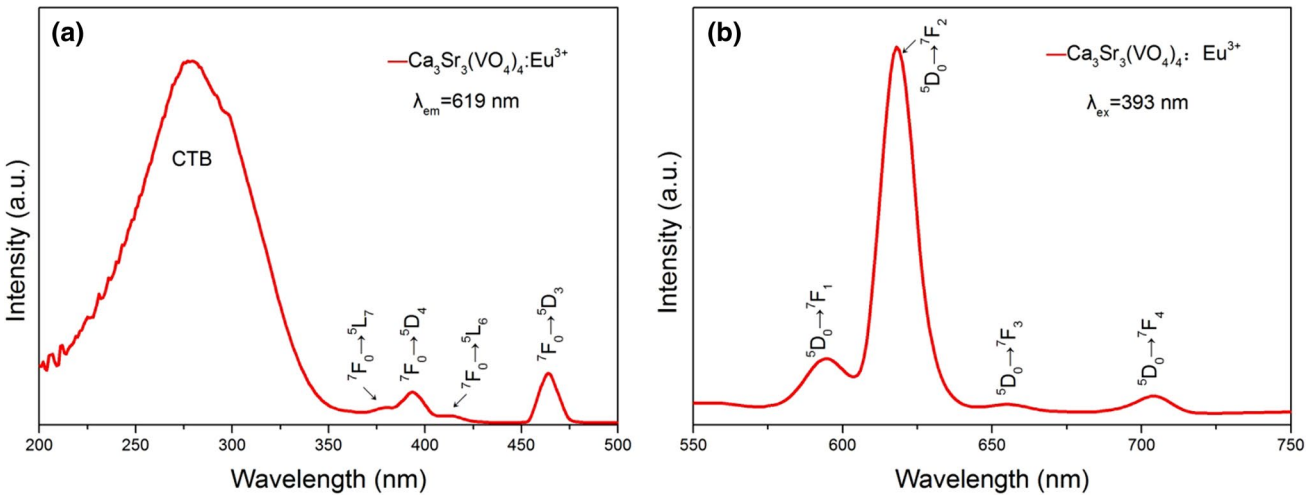

Fig. 5 **a** Excitation and **b** emission spectra of the $Ca_3Sr_3(VO_4)_4$:Eu^{3+} phosphor

intense peak in the UV–NUV region was located at 393 nm, which represents the $^7F_0 \rightarrow {}^5L_6$ transition of Eu^{3+}. Figure 6 shows the emission spectra of different concentrations of Eu^{3+} single-doped $Ca_3Sr_3(VO_4)_4$ phosphors. It is evident that the emission intensity of Eu^{3+} single-doped $Ca_3Sr_3(VO_4)_4$ phosphors consistently increased with increasing percentage of Eu^{3+} up to 5 mol%, and then declined when the concentration of Eu^{3+} was above 5 mol%. Consequently, $Ca_3Sr_3(VO_4)_4$:0.05Eu^{3+} exhibited the strongest emission intensity.

The luminescence characteristics of $Ca_3Sr_3(VO_4)_4$:Sm^{3+} were also investigated and the results are shown in Fig. 7. The emission spectrum show four emission peaks located at 565, 605, 651, and 712 nm upon excitation at 393 nm.

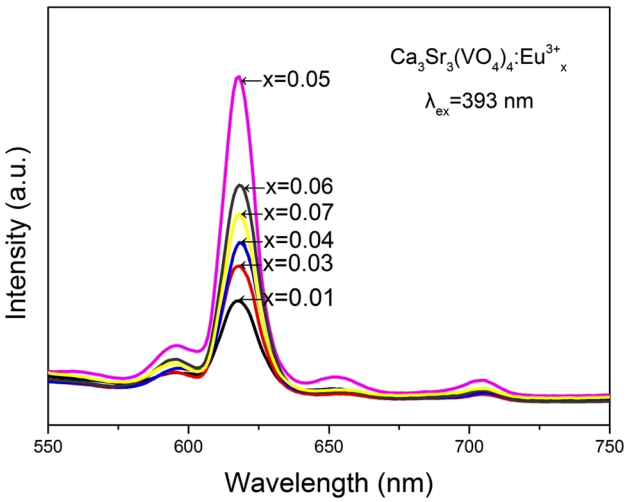

Fig. 6 Emission spectra of $Ca_3Sr_3(VO_4)_4$:xEu^{3+} with various values of x

The highest peak centered at approximately 605 nm is due to the $^4G_{5/2} \rightarrow {}^6H_{7/2}$ transition of Sm^{3+}. Meanwhile, the three other peaks at 565, 651, and 712 nm were ascribed to the $^4G_{5/2} \rightarrow {}^6H_{5/2}$, $^4G_{5/2} \rightarrow {}^6H_{9/2}$, and $^4G_{5/2} \rightarrow {}^6H_{11/2}$ transitions of Sm^{3+}, respectively. Upon monitoring the $^4G_{5/2} \rightarrow {}^6H_{7/2}$ transition of Sm^{3+}, the PLE spectrum was made up of a CTB from 200 to 350 nm and some sharp peaks extending from 350 to 500 nm; these small peaks were attributed to the electronic transitions of $^6H_{5/2} \rightarrow {}^4L_{17/2}$ (361 nm), $^6H_{5/2} \rightarrow {}^6P_{5/2}$ (376 nm), $^6H_{5/2} \rightarrow {}^4F_{7/2}$ (405 nm), $^6H_{5/2} \rightarrow ({}^6P,{}^4P)_{5/2}$ (416 nm), $^6H_{5/2} \rightarrow {}^4G_{9/2}$ (439 nm), and $^6H_{5/2} \rightarrow {}^4I_{11/2}$ (476 nm). The most intense peak was that located at 405 nm.

3.3 Photoluminescence spectra of Eu^{3+} and Sm^{3+} co-doped $Ca_3Sr_3(VO_4)_4$

Based on the analysis of the photoluminescence properties of Eu^{3+} and Sm^{3+} single-doped $Ca_3Sr_3(VO_4)_4$, Sm^{3+} and Eu^{3+} co-doped $Ca_3Sr_3(VO_4)_4$ samples were synthesized and their photoluminescence properties were analyzed. The emission spectra of $Ca_3Sr_3(VO_4)_4$:0.05Eu^{3+}, $y$$Sm^{3+}$ ($y = 0$, 0.01, 0.03, 0.05, 0.07, 0.09, 0.11) are shown in Fig. 8. The emissions from the $^5D_0 \rightarrow {}^7F_2$ transition of Eu^{3+} and the $^4G_{5/2} \rightarrow {}^6H_{9/2}$ transition of Sm^{3+} are changed similar with Sm^{3+} increasing when excited at 393 nm. This supports the theory that Sm^{3+} can transfer the absorbed energy to Eu^{3+}. Moreover, the PL intensity of the Sm^{3+} and Eu^{3+} co-doped phosphors at 619 nm was much higher than samples without Sm^{3+} doping, confirming that the 393 nm excitation energy can be absorbed by Sm^{3+} and then subsequently transferred to Eu^{3+}. Upon fixing the Eu^{3+} concentration at 5 mol% and increasing the Sm^{3+} concentration to 9 mol%, the luminescence intensity reached its maximum, and decreased at higher or lower concentrations of Sm^{3+}. This phenomenon

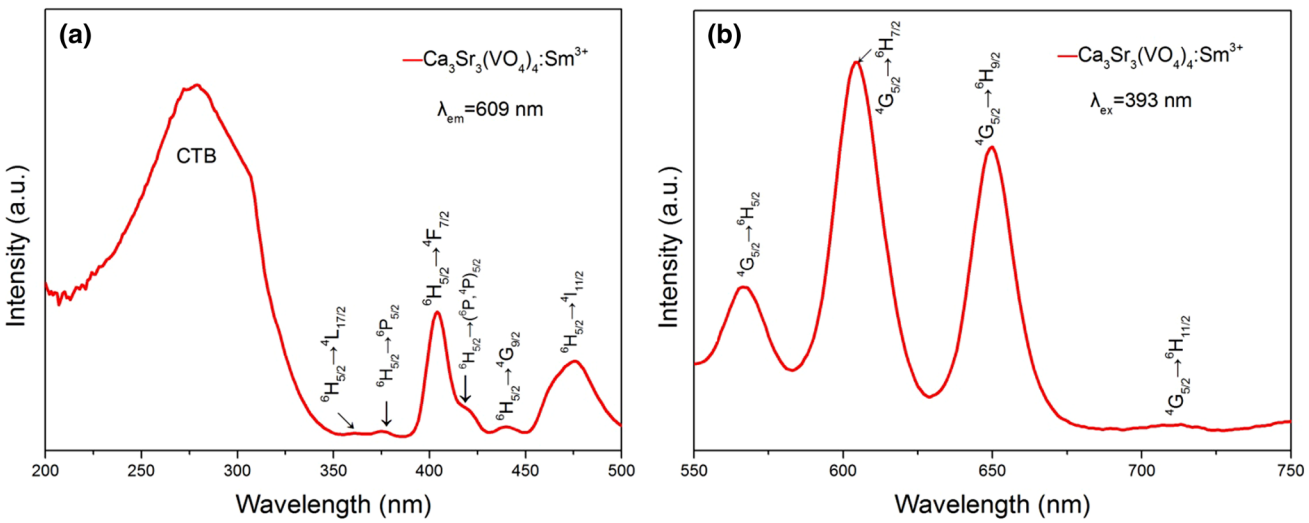

Fig. 7 **a** Excitation and **b** emission spectra of the $Ca_3Sr_3(VO_4)_4$:Sm^{3+} phosphor

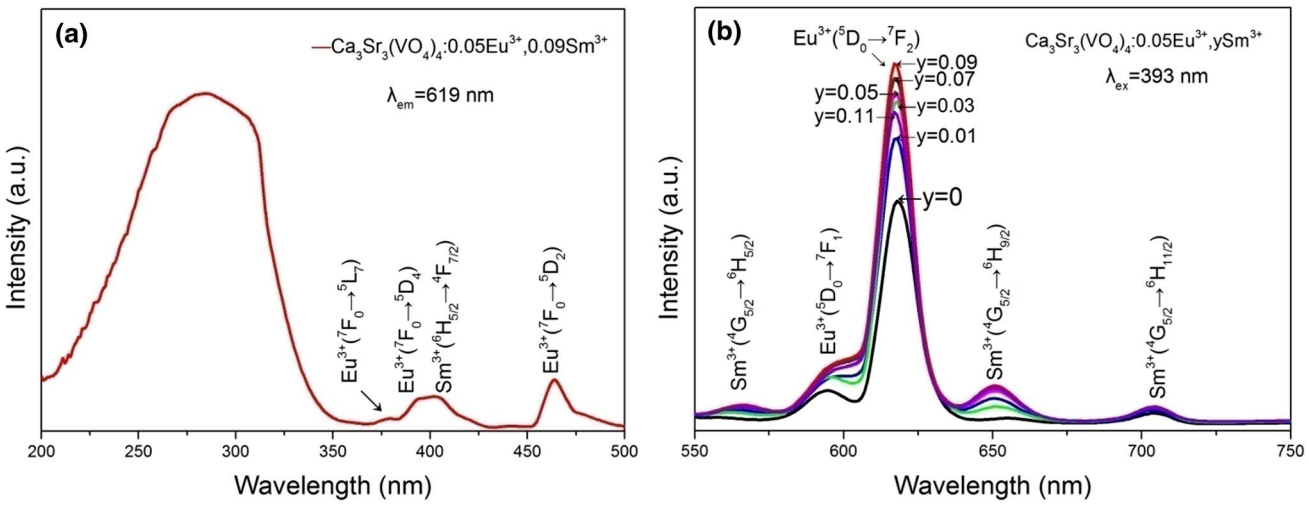

Fig. 8 **a** Excitation spectrum of $Ca_3Sr_3(VO_4)_4$:0.05Eu^{3+}, 0.09Sm^{3+} with monitoring at 619 nm, and **b** emission spectra of $Ca_3Sr_3(VO_4)_4$:0.05Eu^{3+}, ySm^{3+} ($0 \le y \le 0.11$) upon excitation at 393 nm

can be explained by the concentration quenching effect because Sm^{3+} can transfer energy to different sites of Sm^{3+} in the host lattice [18].

In this research, all of the Eu^{3+} and Sm^{3+} co-doped $Ca_3Sr_3(VO_4)_4$ phosphors can transmit bright red light if using UV or NUV lights as the excitation source. As Fig. 8 shows, the PLE spectrum monitoring the emission at 619 nm consisted of many excitation peaks in the range of 350–500 nm, which were located at 380, 393, 405, and 464 nm, corresponding to the $^7F_0\rightarrow{}^5L_7$ transition of Eu^{3+}, the $^7F_0\rightarrow{}^5L_6$ transition of Eu^{3+}, the $^6H_{5/2}\rightarrow{}^4F_{7/2}$ transition of Sm^{3+}, and the $^7F_0\rightarrow{}^5D_2$ transition of Eu^{3+}, respectively. It can be observed that the excitation spectrum of the Sm^{3+} and Eu^{3+} co-doped $Ca_3Sr_3(VO_4)_4$ phosphor was remarkably different from the samples without Sm^{3+} doping, because there is a new excitation peak located at approximately 405 nm. Meanwhile, this co-doped phosphor also has a CTB from 200 to 350 nm that is centered at 285 nm, which is mainly due to the allowed transition $^1A_1\rightarrow{}^1T_2$ with the CTS of VO^{3-} [26]. Meanwhile, we cannot exclude the existence of CTB of $Sm^{3+}\rightarrow O^{2-}$ and $Eu^{3+}\rightarrow O^{2-}$ in the spectrum, as these CTBs are also situated in this region [27]. Upon excitation at 393 nm, the emission spectra consist of four main emission peaks at 565, 594, 619, 651, and 705 nm, which correspond to the $^4G_{5/2}\rightarrow{}^6H_{5/2}$ of Sm^{3+}, $^5D_0\rightarrow{}^7F_1$ of Eu^{3+}, $^5D_0\rightarrow{}^7F_2$ of Eu^{3+}, $^4G_{5/2}\rightarrow{}^6H_{9/2}$ of Sm^{3+}, and $^4G_{5/2}\rightarrow{}^6H_{11/2}$ of Sm^{3+}, respectively. The highest emission peak, which is located at 619 nm, is due to a transition of Eu^{3+}. As shown in Fig. 9, by comparing Eu^{3+} and Sm^{3+} co-doped samples and single-doped samples with the same concentration of Eu^{3+} and under otherwise identical conditions, it is obvious that the Sm^{3+} single-doped sample had no emission intensity at 619 nm

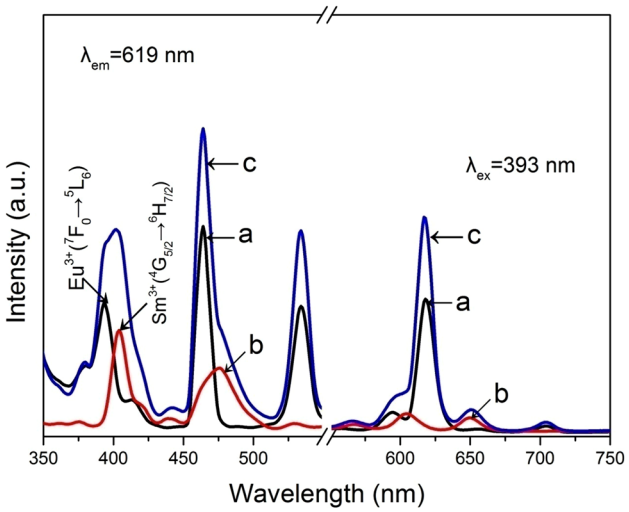

Fig. 9 Photoluminescence spectra of Eu^{3+} and Sm^{3+} single-doped and co-doped $Ca_3Sr_3(VO_4)_4$ phosphors: **a** $Ca_3Sr_3(VO_4)_4$:0.05Eu^{3+}, **b** $Ca_3Sr_3(VO_4)_4$:0.05Sm^{3+}, **c** $Ca_3Sr_3(VO_4)_4$:0.05Eu^{3+}, 0.05Sm^{3+}

but exhibited its strongest emission peak at 609 nm under excitation at 393 nm, whereas the emission intensity of the $Ca_3Sr_3(VO_4)_4$:Eu^{3+}, Sm^{3+} phosphor at 619 nm was much stronger than that of the $Ca_3Sr_3(VO_4)_4$:Eu^{3+} phosphor, which proves that the luminescence mechanism of the Eu^{3+} and Sm^{3+} co-doped $Ca_3Sr_3(VO_4)_4$ phosphor consists of Eu^{3+} luminescence and Sm^{3+} passing energy to Eu^{3+}. The excitation peak at 405 nm can be divided into two excitation peaks by using Gaussian fitting, owing to the peak of the $^7F_0\rightarrow{}^5L_6$ transition of Eu^{3+} partially overlapping with the peak of the $^4G_{5/2}\rightarrow{}^6H_{7/2}$ transition of Sm^{3+}. That is, the excitation of Eu^{3+}-doped samples

around 393 nm can be broadened and strengthened by co-doping with Sm^{3+}, which is beneficial for application to NUV LEDs.

The lifetime of $Eu^{3+:5}D_0$ and $Sm^{3+:4}G_{5/2}$ with varying Sm^{3+} content is shown in Fig. 10a, b respectively. The monitoring wavelength is at 619 and 609 with a 393 nm excitation. The decay curves of $Ca_3Sr_3(VO_4)_4$:0.05Eu^{3+}, ySm^{3+} ($0 \le y \le 0.11$) phosphors are well fitted by the second order exponential function:

$$y = y_0 + A_1 \exp\left(\frac{-x - x_0}{\tau_1}\right) + A_2 \exp\left(\frac{-x - x_0}{\tau_2}\right) \quad (4)$$

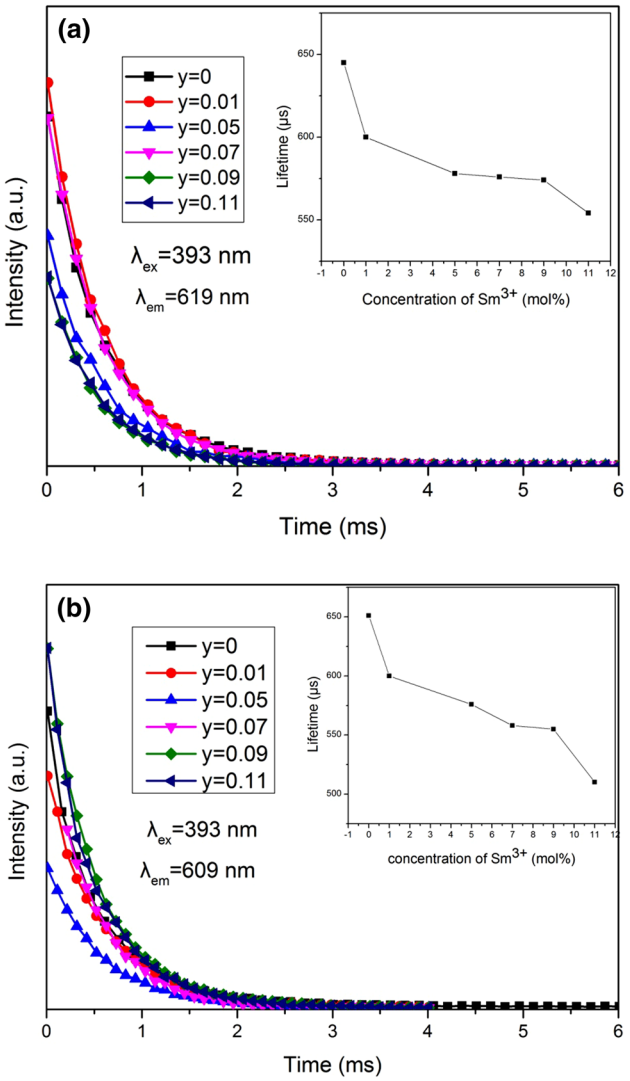

Fig. 10 **a** The decay curves of $Ca_3Sr_3(VO_4)_4$:0.05Eu^{3+}, ySm^{3+} ($0 \le y \le 0.11$) phosphors ($\lambda_{ex} = 393$ nm and $\lambda_{em} = 619$ nm) and the relation between lifetime and Sm^{3+} ion doping concentration. **b** The decay curves of $Ca_3Sr_3(VO_4)_4$:0.05Eu^{3+}, ySm^{3+} ($0 \le y \le 0.11$) phosphors ($\lambda_{ex} = 393$ nm and $\lambda_{em} = 609$ nm) and the relation between lifetime and Sm^{3+} ion doping concentration

where τ_1, and τ_2 are the luminescence decay times. The value of decay time can be calculated by the following equation [24]:

$$\tau = \frac{(A_1\tau_1^2 + A_2\tau_2^2)}{(A_1\tau_1 + A_2\tau_2)} \quad (5)$$

It can be seen from Fig. 10 that the lifetime of $Ca_3Sr_3(VO_4)_4$:0.05Eu^{3+}, ySm^{3+} ($0 \le y \le 0.11$) phosphors decreases with increasing of Sm^{3+} from 0 to 11 mol%. The result indicates that energy transfer occurs between Eu^{3+} and Sm^{3+} ions.

Figure 11 shows the energy transfer process between Sm^{3+} and Eu^{3+}. As discussed previously, when the excitation wavelength is 393 nm, Sm^{3+} can be excited from its ground state $^6H_{15/2}$ to its corresponding excited state $^4F_{7/2}$, and Eu^{3+} can be excited from its ground state $^7F_0$ to its corresponding excited state $^5L_6$. After the excited electrons of Eu^{3+} and Sm^{3+} return to their respective ground states, the Sm^{3+} can transfer its absorbed energy to the Eu^{3+}. Furthermore, a channel that can transfer energy between the $^4G_{5/2}$ energy level of Sm^{3+} and the $^5D_0$ energy level of Eu^{3+} exists, because these two energy levels are very close. The $^4F_{7/2}$ energy level of Sm^{3+} can be reached upon excitation with 393 nm NUV light, and the excited electron of Sm^{3+} automatically returns to its lowest excited energy level $^4G_{5/2}$. Subsequently, energy transfer can occur between the $^4G_{5/2}$ level of Sm^{3+} and the $^5D_0$ level of Eu^{3+} by resonance. This explains why the emission is improved in the Eu^{3+} and Sm^{3+} co-doped $Ca_3Sr_3(VO_4)_4$ phosphor. One of the decay channels of Sm^{3+} can be described as follows [18]:

$$\frac{1}{\tau_s} = \frac{1}{\tau_{s0}} + P_{NR} + P_T \quad (6)$$

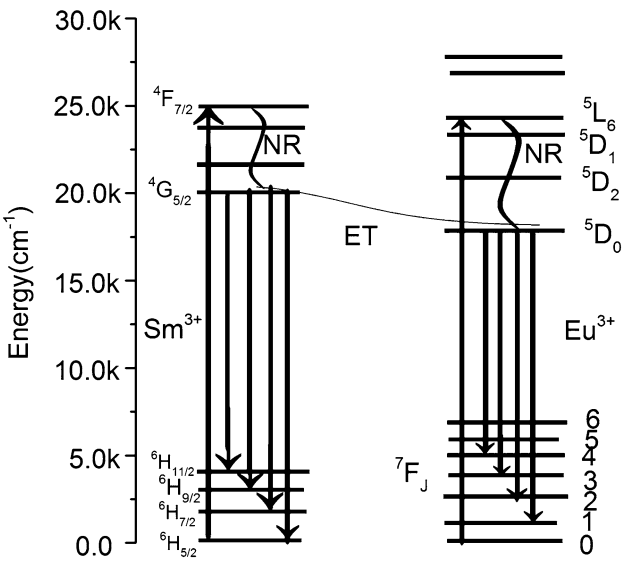

Fig. 11 Energy level diagram for the energy transfer process between Sm^{3+} and Eu^{3+} ions

where τ_s is the lifetime of the sensitizer in the presence of the activator, τ_{s0} is the lifetime of sensitizer in the absence of the activator, P_{NR} is the probability of nonradiative transitions, and P_T is the probability that Sm^{3+} can transfer energy to Eu^{3+}. Exchanging τ_s/τ_{s0} for I_s/I_{s0} and taking no account of the influence of P_{NR}, the efficiency of the energy transfer from Sm^{3+} to Eu^{3+} can be described as follows:

$$\eta_T = 1 - \frac{I_s}{I_{s0}} \tag{7}$$

where I_{s0} is the luminescence intensity of the sensitizer in the absence of the activator Eu^{3+}, which can be measured from the emission intensity of $Ca_3Sr_3(VO_4)_4$:$0.09Sm^{3+}$ at 651 nm, and I_s is the luminescence intensity of the sensitizer in the presence of the activator Eu^{3+}, which can be measured from the emission intensity of $Ca_3Sr_3(VO_4)_4$:$0.05Eu^{3+}$, $0.09Sm^{3+}$ at 651 nm. According to this approach, the energy transfer efficiency of the optimal sample is 37%. For the purpose of confirming the type of interaction between Sm^{3+} and Eu^{3+}, we calculated the distance between Sm^{3+} and Eu^{3+} using the following equation:

$$R_{Sm-Eu} = 2\left[\frac{3V}{4\pi zN}\right]^{\frac{1}{3}} \tag{8}$$

where V is the volume of the unit cell (4085.8 $Å^3$), which can be obtained from the refinement result, z is the sum concentration of Eu^{3+} and Sm^{3+}, and N ($N = 10.5$) is the number of $Ca_3Sr_3(VO_4)_4$ ions in the unit cell. According to this equation, the distance between Eu^{3+} and Sm^{3+} in the various co-doped $Ca_3Sr_3(VO_4)_4$:$0.05Eu^{3+}$, ySm^{3+} phosphors ($y = 0.01$, 0.03, 0.05, 0.07, 0.09, 0.11) was estimated to be 23.14, 21.02, 19.52, 18.37, 17.45, and 16.68 nm, respectively. However, the typical critical distance of the exchange interaction between Eu^{3+} and Sm^{3+} is 0.5 nm, which is much smaller than the distance between Eu^{3+} and Sm^{3+} in the co-doped samples. Under normal conditions, the exchange interaction, multipole interaction, and radiation reabsorption may occur by transferring nonradiative energy among different ions [28]. To sum up, the exchange interaction hardly occurred during the process of energy transfer between Sm^{3+} and Eu^{3+} in the host lattice. In addition to this, a broad overlap of fluorescence activator and sensitizer can induce the radiation absorption. Considering the spectral characteristics of the co-doped samples, the type of energy transfer should be multipole interaction. What is more, based on the energy level difference, the phonon assisted energy transfer can be also occurred.

The emission spectra of $Ca_3Sr_3(VO_4)_4$:$0.05Eu^{3+}$, $Ca_3Sr_3(VO_4)_4$:$0.05Eu^{3+}$, $0.09Sm^{3+}$, and the commercial phosphor Y_2O_3:$0.05Eu^{3+}$ at an excitation wavelength of 393 nm were compared, as shown in Fig. 12. It is clear that the PL intensity of $Ca_3Sr_3(VO_4)_4$:$0.05Eu^{3+}$ was much lower than that of $Ca_3Sr_3(VO_4)_4$:$0.05Eu^{3+}$, $0.09Sm^{3+}$, and the integrated PL intensity of $Ca_3Sr_3(VO_4)_4$:$0.05Eu^{3+}$, $0.09Sm^{3+}$ ranging from 550 to 750 nm was improved by about 1.6 times compared to that of $Ca_3Sr_3(VO_4)_4$:$0.05Eu^{3+}$. The integrated emission intensities of $Ca_3Sr_3(VO_4)_4$:$0.05Eu^{3+}$, $0.09Sm^{3+}$ and commercial Y_2O_3:$0.05Eu^{3+}$ were also compared, which revealed that the integrated emission intensity of $Ca_3Sr_3(VO_4)_4$:$0.05Eu^{3+}$, $0.09Sm^{3+}$ was enhanced by around 2.4 times compared to that of Y_2O_3:$0.05Eu^{3+}$ in the 550–750 nm range. In addition, the quantum efficiency of $Ca_3Sr_3(VO_4)_4$:$0.05Eu^{3+}$, $Ca_3Sr_3(VO_4)_4$:$0.05Eu^{3+}$, $0.09Sm^{3+}$, and the commercial phosphor Y_2O_3:$0.05Eu^{3+}$ were also compared in Table 1, the results show that $Ca_3Sr_3(VO_4)_4$:$0.05Eu^{3+}$, $0.09Sm^{3+}$ has the highest quantum efficiency. This comparison leads to the conclusion that the $Ca_3Sr_3(VO_4)_4$:$0.05Eu^{3+}$, $0.09Sm^{3+}$ phosphor has excellent photoluminescence properties for application in white-light-emitting diodes.

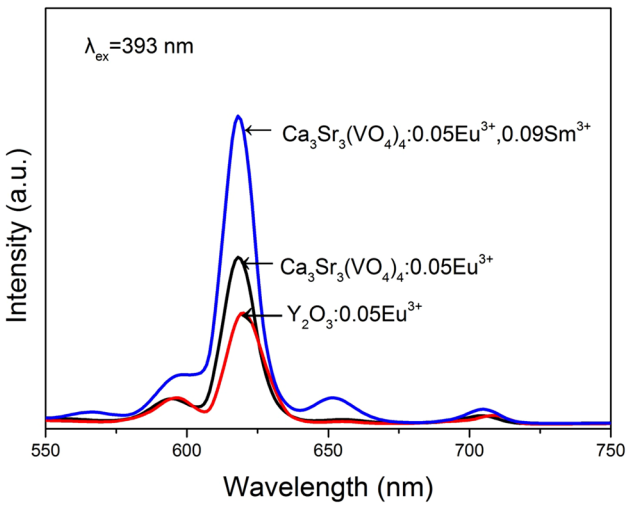

Fig. 12 Emission spectrum of $Ca_3Sr_3(VO_4)_4$:$0.05Eu^{3+}$, $Ca_3Sr_3(VO_4)_4$:$0.05Eu^{3+}$, $0.09Sm^{3+}$, and commercial Y_2O_3:$0.05Eu^{3+}$ phosphors

Table 1 The quantum efficiency of $Ca_3Sr_3(VO_4)_4$:$0.05Eu^{3+}$, $Ca_3Sr_3(VO_4)_4$:$0.05Eu^{3+}$, $0.09Sm^{3+}$, and the commercial phosphor Y_2O_3:$0.05Eu^{3+}$

Phosphor	Y_2O_3:$0.05Eu^{3+}$	$Ca_3Sr_3(VO_4)_4$:$0.05Eu^{3+}$	$Ca_3Sr_3(VO_4)_4$:$0.05Eu^{3+}$,$0.09Sm^{3+}$
Quantum efficiency	0.43%	1.45%	2.77%

Figure 13 shows the CIE chromaticity coordinates of the National Television System Committee (NTSC) standard for red phosphors ($x=0.67$, $y=0.33$) compared with $Ca_3Sr_3(VO_4)_4$:0.05Eu^{3+} (0.6448, 0.3548), commercial Y_2O_3:0.05Eu^{3+} (0.649, 0.343), and $Ca_3Sr_3(VO_4)_4$:0.05Eu^{3+}, 0.09Sm^{3+} (0.6595, 0.3402). These values indicate that the CIE chromaticity coordinate of $Ca_3Sr_3(VO_4)_4$:0.05Eu^{3+}, 0.09Sm^{3+} is closer to the NTSC standard for red phosphors than other commercial phosphors. The Eu^{3+} and Sm^{3+} co-doped $Ca_3Sr_3(VO_4)_4$ phosphor could be used as a potential red-emitting phosphor for application in near-UV or blue-based white LEDs.

4 Conclusion

A series of $Ca_3Sr_3(VO_4)_4$:Eu^{3+} and $Ca_3Sr_3(VO_4)_4$:Eu^{3+},Sm^{3+} phosphors were synthesized by a citric acid assisted sol combustion method. After firing for 1 h, all samples were matched perfectly to $Ca_3Sr_3(VO_4)_4$ (PDF card: JCPDS 52-0468), which has a rhombohedral structure and belongs to the space group of *R*3*c*. The photoluminescence properties of Eu^{3+} and Sm^{3+} single-doped and co-doped $Ca_3Sr_3(VO_4)_4$ phosphors in the near-UV region were investigated. As a sensitizer, Sm^{3+} absorbs the excitation energy and transfers it to the Eu^{3+} ions. The integrated intensity of the optimal sample $Ca_3Sr_3(VO_4)_4$:0.05Eu^{3+}, 0.09Sm^{3+} was enhanced to 1.6 times and 2.4 times compared to $Ca_3Sr_3(VO_4)_4$:0.05Eu^{3+} and Y_2O_3:0.05Eu^{3+}, respectively, indicating that it possesses excellent photoluminescence properties for application to NUV LEDs. Furthermore, the CIE chromaticity coordinate of $Ca_3Sr_3(VO_4)_4$:0.05Eu^{3+}, 0.09Sm^{3+} was found to be closer to standard for red light than other commercial phosphors. Moreover, this research proves that Sm^{3+} can be employed to broaden and strengthen the absorption around 393 nm for Eu^{3+}-doped samples. Finally, the Sm^{3+} and Eu^{3+} co-doped $Ca_3Sr_3(VO_4)_4$ phosphors may be applied as potential red-emitting luminescent materials for white-lighting devices under UV or NUV excitation.

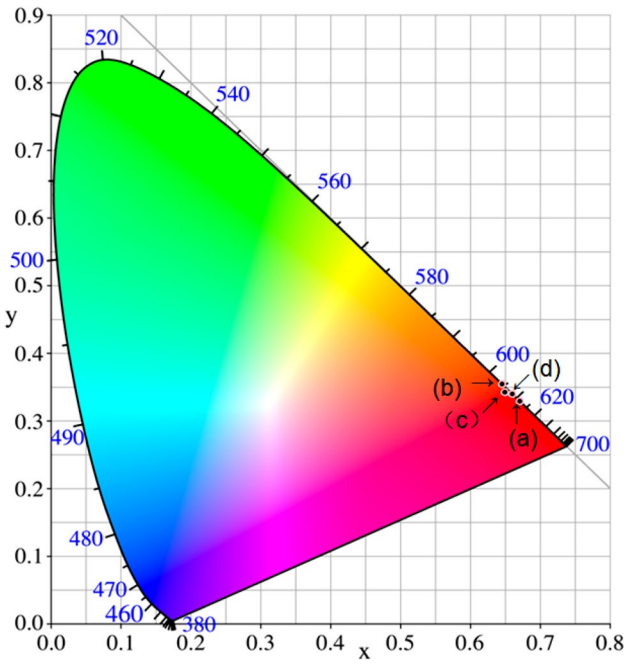

Fig. 13 CIE chromaticity coordinates of **a** the NTSC standard for red phosphors ($x=0.67$, $y=0.33$), (b) $Ca_3Sr_3(VO_4)_4$:0.05Eu^{3+}, (c) commercial Y_2O_3:0.05Eu^{3+}, and (d) $Ca_3Sr_3(VO_4)_4$:0.05Eu^{3+}, 0.09Sm^{3+}

Acknowledgements We would like to acknowledge the financial support from the Key Scientific and Technological Research and Development Program (Grant No. 2017GZ0400), Sichuan Province, P.R. China.

References

1. C. Michail, N. Kalyvas, I. Valais, S. David, I. Seferis, A. Toutountzis, A. Karabotsos, P. Liaparinos, G. Fountos, I. Kandarakis, On the response of $GdAlO_3$: Ce powder scintillators. J. Lumin. **144**, 45–52 (2013)
2. G.C. Brainard, W. Coyle, M. Ayers, J. Kemp, B. Warfield, J. Maida, C. Bowen, C. Bernecker, S. Lockley, J.P. Hanifin, Solid-state lighting for the International Space Station: tests of visual performance and melatonin regulation. Acta Astronaut. **92**, 21–28 (2013)
3. K.J. Chen, H.C. Chen, C.C. Lin, C.H. Wang, C.C. Yeh, H.H. Tsai, S.H. Chien, M.H. Shih, H.C. Kuo, An investigation of the optical analysis in white light-emitting diodes with conformal and remote phosphors structure. J. Display Technol. **9**, 915–920 (2013)
4. L. Chen, C.-C. Lin, C.-W. Yeh, R.-S. Liu, Light converting inorganic phosphors for white light-emitting diodes. Materials **3**, 2172–2195 (2010)
5. J. Zhang, W. Zhuang, X. Xing, L. Wang, Y. Li, Y. Zheng, Y. Liu, Y. Hu, Blue-shift of spectrum and enhanced luminescent properties of YAG:Ce^{3+} phosphor induced by small amount of La^{3+} incorporation. J. Alloys Compd. **674**, 93–97 (2016)
6. H.-J. Reyher, N. Hausfeld, M. Pape, J. Baur, J. Schneider, Attribution of the near-UV absorption bands of YAG:Ce to Ce^{3+}-ions by MCD and ODMR. Solid State Commun. **110**, 345–349 (1999)
7. Y. Pan, M. Wu, Q. Su, Tailored photoluminescence of YAG:Ce phosphor through various methods. J. Phys. Chem. Solids **65**, 845–850 (2004)
8. J. Liu, Z.C. Wu, S.P. Kuang, White-light from NUV InGaN LED chip precoated with blue/yellow phosphors. Optoelectron. Advan. Mater.-Rapid Commun. **7**, 343–345 (2013)
9. X. Zhang, Y. Chen, L. Zhou, M. Gong, NUV chip based white LED using thermal stable Eu^{2+}-activated phosphors and borate phosphor. Mater. Lett. **93**, 390–392 (2013)
10. H. Wu, X.M. Zhang, C.F. Guo, R. Xu, M.M. Wu, Q. Su, Three-band white light from InGaN-based blue LED chip precoated with green/red phosphors. IEEE Photonics Technol. Lett. **17**, 1160–1162 (2005)
11. V. Sivakumar, U.V. Varadaraju, An orange-red phosphor under near-UV excitation for white light emitting diodes. J. Electrochem. Soc. **154**, J28–J31 (2007)
12. Z.L. Wang, H.B. Liang, L.Y. Zhou, H. Wu, M.L. Gong, Q. Su, Luminescence of (Li0.333Na0.334K0.333) $Eu(MoO_4)_2$ and its application in near UV InGaN-based light-emitting diode. Chem. Phys. Lett. **412**, 313–316 (2005)

13. A. Huignard, T. Gacoin, J.P. Boilot, Synthesis and luminescence properties of colloidal YVO_4:Eu phosphors, Chemistry of Materials. 12 (2000) 1090–1094
14. S. Neeraj, N. Kijima, A.K. Cheetham, Novel red phosphors for solid state lighting; the system $Bi_{(x)}Ln_{(1-x)}VO_{(4)}$:$Eu^{3+}$/$Sm^{3+}$ (Ln = Y, Ga). Solid State Commun. **131**, 65–69 (2004)
15. A.R. Dhobale, M. Mohapatra, V. Natarajan, S.V. Godbole, Synthesis and photoluminescence investigation of the white light emitting phosphor, vanadate garnet, $Ca_2NaMg_2V_3O_{12}$ co-doped with Dy and Sm. J. Lumin. **132**, 293–298 (2012)
16. S. Choi, Y.M. Moon, K. Kim, H.K. Jung, S. Nahm, Luminescent properties of a novel red-emitting phosphor: Eu^{3+}-activated $Ca_3Sr_3(VO_4)_4$. J. Lumin. **129**, 988–990 (2009)
17. J. Sun, R. Sun, J. Sun, H. Du, Photoluminescence studies on a new red emitting Sm^{3+}-doped alkaline-earth vanadate phosphors $Ca_3Sr_3(VO_4)_4$:Sm^{3+}, Na^{3+}. Optoelectron. Adv. Mater.-Rapid Commun. **5**, 215–219 (2011)
18. A. Senouci, J. Frene, H. Zaidi, Wear mechanism in graphite–copper electrical sliding contact. Wear **225–229**, 949–953 (1999)
19. F. Zhang, W. Zhang, Z. Zhang, Y. Huang, Y. Tao, Luminescent characteristics and energy transfer of a red-emitting YVO_4:Sm^{3+}, Eu^{3+} phosphor. J. Lumin. **152**, 160–164 (2014)
20. M. Ye, G. Zhou, L Zhou, D. Lu, Y. Li, X. Xiong, K. Yang, M. Chen, Y. Pan, P. Wu, Z. Wang, H. Liu, Q. Xia, Luminescent properties and energy transfer process of Sm^{3+}-Eu^{3+} co-doped $MY_2(MoO_4)_4$ (M = Ca, Sr and Ba) red-emitting phosphors. Solid State Sci. **59**, 44e51 (2016)
21. K. Qiu, J. Li, J. Li, X. Lu, Y. Gong, J. Li, Luminescence property of $Ca_3(VO_4)_2$:Eu^{3+} dependence on molar ratio of Ca/V and solution combustion synthesis temperature. J. Mater. Sci. **45**, 5456–5462 (2010)
22. K. Tonooka, O. Nishimura, Effect of calcinations temperature on the luminescent properties of Tb-doped borosilicate glasses. J. Mater. Sci. **34**, 5039–5044 (1999)
23. I. Ahemen, F.B. Dejene, B. Viana, P. Aschehoug, E. Odoh, Effect of annealing temperature and ambient on the structure and optical properties of Eu^{3+}-doped ZnS nanocrystals. Mater. Chem. Phys. **184**, 250–260 (2016)
24. M. Vijayakumar, K. Mahesvaran, D.K. Patel, S. Arunkumar, K. Marimuthu, Structural and optical properties of Dy^{3+} doped aluminofluoroborophosphate glasses for white light applications. Opt. Mater **37**, 695–705 (2014)
25. Y. Zeng, K. Qiu, Z. Yang, Y. Bu, W. Zhang, J. Li, Enhanced red emission of $NaSrVO_4$:Eu^{3+} phosphor via Bi^{3+}co-doping for the application to white LEDs. Ceram. Int. **43**, 830–834 (2017)
26. K.Y. Kim, S.J. Yoon, K. Park, Synthesis and photoluminescence properties of red-emitting $Ca_{3-3x/2}(VO_4)_2$:xEu^{3+} phosphors. J. Lumin. **160**, 78–84 (2015)
27. F. Zhang, Y. Wang, Y. Tao, VUV spectroscopic properties of $Ba_2Gd_2Si_4O_{13}$:Re^{3+}(Re^{3+}=Ce^{3+}, Tb^{3+}, Dy^{3+}, Eu^{3+}, Sm^{3+}). Mater. Res. Bull. **48**, 1952–1956 (2013)
28. J. Su, X. Mi, J. Sun, L. Yang, C. Hui, L. Lu, Z. Bai, X. Zhang, Tunable luminescence and energy transfer properties in YVO_4:Bi^{3+}, Eu^{3+} phosphors. J. Mater. Sci. **52**, 782–792 (2017)